Research Article

Effect of 3D Printing Parameters on the Refractive Index, Attenuation Coefficient, and Birefringence of Plastics in Terahertz Range

Alexander T. Clark [ID], John F. Federici [ID], and Ian Gatley [ID]

Department of Physics, New Jersey Institute of Technology, 323 Dr. M.L.King. Jr. Blvd., Newark, NJ, USA

Correspondence should be addressed to John F. Federici; federici@njit.edu

The refractive indices, attenuation coefficients, and level of birefringence of various 3D printing plastics may change depending on the printing parameters. Transmission terahertz time-domain spectroscopy was used to look for such effects in Copolyester (CPE), Nylon, Polycarbonate (PC), Polylactic acid, and Polypropylene. The thickness of each sample was measured using an external reference structure and time-of-flight measurements. The parameters varied were printer nozzle size, print layer height, and print orientation. Comparison of these parameters showed that a printer's nozzle size and print layer height caused no change in real refractive index or attenuation coefficient. A change in printing orientation from vertical to horizontal caused an increase both in real refractive index and in attenuation coefficient. In vertically printed samples, the increase in birefringence was proportional to the increase in layer height and inversely proportional to nozzle size. There was no measurable intrinsic birefringence in the horizontally printed samples. These effects should be taken into account in the design of FDM 3D printed structures that demand tailored refractive indices and attenuation coefficients, while also providing a foundation for nondestructive evaluation of FDM 3D printed objects and structures.

1. Introduction

Terahertz time-domain spectroscopy (THz-TDS) is increasing in popularity as a method for noncontact and nondestructive material characterization. Terahertz (THz) radiation refers to the electromagnetic waves within the "gap" of frequencies that lie between the microwave and infrared spectrums, which can transmit through nonconductive materials [1]. In the case of THz-TDS, the THz electric field is measured as opposed to its intensity. Applications of THz-TDS nondestructive evaluation include measuring the plasma density output by an atmospheric pressure plasma jet, measuring the degradation of specialty aircraft coatings, and quantifying a glucose level in a diabetic's blood [2–4]. This paper addresses the use of THz-TDS in 3D printing and additive manufacturing (AM).

One industry that has a large potential for benefit from THz-TDS is 3D printing and additive manufacturing (AM).

3D printing has many variables that can affect the quality of the final product. Specifically, fused deposition modeling (FDM) 3D printers, which lay down melted layers of plastic on top of each other to create a final 3D structure, are a natural application of THz-TDS due to the high transparency of plastics to THz radiation. Recently, there have been advances in using FDM printers to print various microwave and terahertz based optical components such as lenses, waveguides, antennas, and fibers [5, 6]. The accuracy and reproducibility of such 3D printed structures will likely depend on the printing parameters, and so the ability to fine-tune properties such as refractive index, attenuation coefficient, and birefringence will depend on detailed knowledge of such dependencies [7]. Specifically, there must be a set standard for the qualification of these parts. Qualification has been recognized by the Federal Government as the largest barrier impeding the progress of 3D printing and AM

to become widely adopted in the manufacturing sector [8–11].

Terahertz optical properties of some 3D printable plastics including Polylactic acid (PLA), Nylon, and Polypropylene (PP) have been previously reported from experiments that did not make reference to the specifics of the printing process. Reference [12] measured the real refractive index as well as the absorption coefficient for various FDM filaments seen in Table 1. These measurements were printing parameter independent and analyzed using the quasispace minimization algorithm which uses the imaginary part of the complex refractive index to calculate its absorption coefficient [12, 13].

Another previous reference reported an absorption coefficient of $10 \, \text{cm}^{-1}$ at 500 GHz for a PLA 3D printed sample [14]. This measurement was once again printing parameter independent and was measured using intensity as opposed to electric field. Various commercially available filaments were analyzed in [15] for their real refractive indices and absorption coefficients using optimized printing parameters. This paper differentiates itself from previous studies by investigating the changes in the refractive index and absorption coefficient in the THz gap using electric field transmission measurements of a 3D printed structure *due to varying printing parameters* used in the 3D printing process. No optical property variations due to changes in printing parameters have been previously reported.

2. Experimental Setup

2.1. Printer, Filaments, and Sample Design. All samples for this research were created using an Ultimaker S5 FDM 3D printer, a widely used commercially available printer controlled by g-code generated by Ultimaker Cura V4.4.1. Each sample was printed using a custom STL model designed in Autodesk Fusion 360. The filament materials used were Copolyester (CPE), Nylon, Polycarbonate (PC), Polylactic acid, and Polypropylene; this is a comprehensive list of the available clear or natural filaments produced by Ultimaker that are compatible with the Ultimaker S5 3D printer. Clear and natural filaments were chosen to avoid the possibility of variations induced by pigments or dyes in the filament that might affect the terahertz measurements.

Each sample measured $20 \times 106 \times 2 \, \text{mm}$, a size large enough to allow measurements to be taken at a variety of locations on each sample, as well as letting ample THz radiation through to obtain proper signal-to-noise ratios. Each sample was measured at three separate locations denoted by the labels A, B, and C corresponding to the tic marks incorporated into the design, as shown in Figure 1. This allowed for consistent measurements for both the thickness of the sample and the refractive index, attenuation coefficient, and birefringence at those locations.

2.2. Printing Parameters. It is common in FDM printing for designs to vary from one another in their choices of infill percentage, printer nozzle size, print layer height, and print orientation. The infill percentage is the amount of repeating

structure printed within the object to create strength and rigidity. Generally, the greater the infill percentage is, the stronger the object becomes due to the increase in the amount of plastic used. For this research, 100% infill was used throughout. Commercially available 3D printers can swap between varieties of nozzle sizes. The nozzle size concomitantly determines the size of the raster (the repeating pattern of parallel lines that are combined to create a 3D object) employed in printing. Nozzle sizes of 0.4 mm and 0.8 mm were used in this experiment. Nozzle size is important for terahertz components because roughness and boundaries will be created differently that may affect the properties of the structure and may need to be removed during a postprocess procedure, such as polishing [16].

The layer height of a print is the thickness of the individual layers laid down by the nozzle during each pass. Layer heights of 0.1 mm, 0.2 mm, and 0.3 mm were used. The layers throughout the structure will be extruded on a certain plane depending on the object's orientation. Horizontal and vertical print orientations were tested, as shown in Figure 2. When the vertical samples were printed, a thicker region routinely formed at the bottom as a consequence of this printing process. This had no effect on the measurements reported here because that thicker part of the sample was not within the regions measured. The terahertz beam was always perpendicular to the front face of the sample during the THz-TDS transmission measurements. A set of standard printing parameters were established. The parameters were a 0.4 mm nozzle, 0.2 mm layer height, a horizontal printing orientation, and Cura recommended heat and speed settings based on the filament used for that sample. The printing speed and temperature employed were those recommended by the manufacturer for optimal printing results.

2.3. Terahertz System and Calculations. A Terametrix T-Ray 5000 THz-TDS instrumentation platform was used to measure the thickness, the real index of refraction, attenuation coefficient, and birefringence of the printed materials. The thickness of the printed samples was determined from time-of-flight delay measurements [17] using an external reference structure (ERS). As shown in Figure 3, the ERS consists of a partially reflecting surface on the left and a metal surface on the right. When a terahertz pulse interacts with the structure, two main pulses are reflected: these correspond to the reflection from the backside of the partially reflecting surface and from the metal, respectively. The time-of-flight difference in the arrival time of the two pulses yields an accurate measurement of the distance between the reflecting surface and the mirror.

Figure 3(a) illustrates the arrival time of pulses called t_1^o and t_4^o in the absence of a sample. The distance between the backside of the reference surface and the front surface of the metal is calculated using time-of-flight to be

$$L_{14} = \frac{c_o \left(t_4^o - t_1^o \right)}{2}. \tag{1}$$

The factor of 2 is present since the terahertz pulse, which reflects from the metal, transmits through the distance L_{14}

TABLE 1: Real refractive index and absorption coefficient at 0.5 THz for various materials [12].

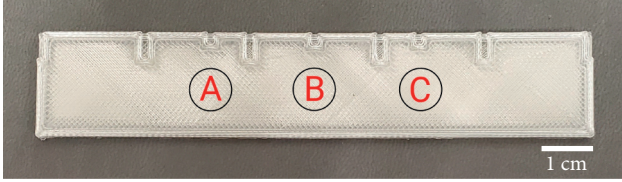| Material	Refractive index (real)	Absorption coefficient (cm^{-1})
PLA	1.89	11
Nylon	1.72	9
PP	1.495	0

FIGURE 1: A single 3D printed sample. A, B, and C correspond to 3 measurement locations, and the circles represent the average terahertz beam size.
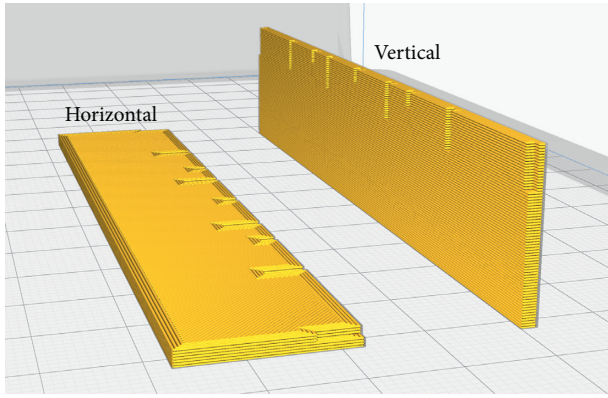

FIGURE 2: Difference in print orientation for the FDM 3D printed samples. "Horizontal" orientation on the left and "vertical" orientation on the right.

twice. When the sample is inserted into the structure, four major peaks are detected in the terahertz waveform. Measuring the timing of each of the four corresponding peaks based on their maximum amplitude identifies the arrival time of the four peaks t_1, t_2, t_3, and t_4. The distances L_{12} and L_{34}, which are calculated from time-of-flight measurements of the pulses, can be subtracted from L_{14} to determine the sample thickness L independent of the refractive index of the sample. The advantage of using this methodology is that the measurement of the thickness L using the propagation time of terahertz pulses is much more accurate than by using calipers. L is then calculated using

$$L = L_{14} - L_{12} - L_{34} = \frac{c_o}{2}\left[\left(t_4^o - t_1^o\right) - \left(t_2 - t_1\right) - \left(t_4 - t_3\right)\right].$$

$$(2)$$

The samples were mounted between the transmitter and receiver perpendicular to the focused terahertz beam. A focused beam was used because the thickness of the samples was well within the Rayleigh range of the setup, while also allowing smaller samples to be used due to the smaller spot size. The beam was focused onto the sample using $1.5''$

diameter, $6''$ focal length, high-density polyethylene aspherical lenses. This allowed for a maximum spot size of 17.1 mm at 100 GHz down to 1.1 mm at 1.5 THz. The samples were held in place using a 3D printed mounting rig, which allowed for consistent and proper alignment within the path of the transmitter and receiver for transmission and the beam splitter for reflection. The refractive indices and attenuation coefficients of the samples were determined from transmission measurements (preferred for moderately transparent and low refractive index samples such as these because the phase variation is integrated over the full thickness of the sample [18]), while birefringence was determined from reflection measurements.

An average over 1000 individual terahertz pulses was taken at each measurement location, resulting in a single output terahertz waveform for the refractive index and attenuation coefficient measurements. This averaged waveform, along with a reference waveform and background waveform, was then transferred into a MATLAB code for analysis. To calculate the real index of refraction as a function of frequency, the corresponding time-domain waveform data must be converted to the frequency domain via a Fourier transform. The phase angles as a function of frequency are calculated for both sample and reference waveforms. The phase difference is used to calculate the frequency-dependent real refractive index (n) using the relationship:

$$n(\nu) = 1 + \frac{c\Delta\phi(\nu)}{2\pi L\nu},$$

$$(3)$$

where c is the speed of light, $\Delta\phi(\nu)$ is the frequency-dependent phase difference, L is the thickness of the sample, and ν is the frequency. Once the frequency-dependent real refractive index has been calculated, it is possible to select a specific frequency at which we compare the real refractive indices and attenuation coefficients of the printed samples with the changes in the various printing parameters.

The analysis of the attenuation coefficient for the 3D printed samples is performed here using measurements of the electric field rather than the intensity. Therefore, relative to the previous quoted results in Table 1 (which have measured the attenuation coefficient in terms of intensity), our attenuation coefficients will be one half those of Table 1. The attenuation coefficient values reported here also take into account reflection losses at the boundaries by calculating the transmission coefficients from air into the printed plastic and from the printed plastic back into air, both at normal incidences, while accounting for changes in sample thickness. Since the plastics are relatively transparent in the terahertz frequency range, the imaginary refractive index is small compared to the real refractive index. In this situation, one can correct the measured amplitude of the transmitted terahertz Fourier transform for Fresnel reflection losses at the air-sample and sample-air interfaces [19]. The imaginary refractive index is calculated from

$$n_i = \frac{c}{2\pi\nu L}\ln\left(\frac{|E_R(\nu)|}{|E_S(\nu)|}t_{12}t_{21}\right),$$
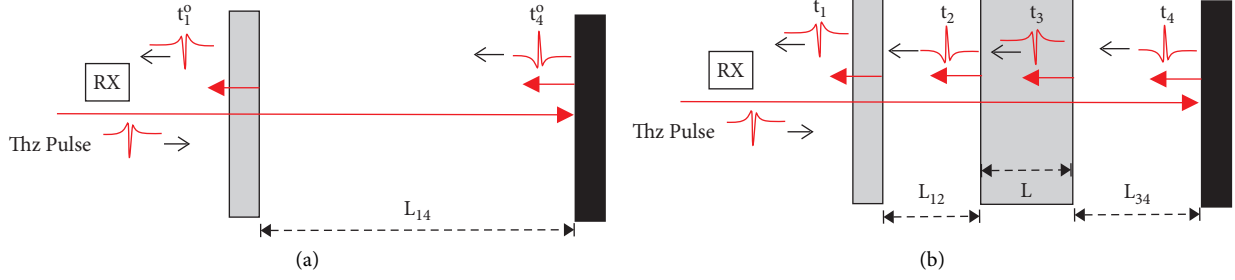
$$(4)$$

FIGURE 3: Illustration of the external reference structure for simultaneous determination of sample thickness. (a) Configuration for determining distance $(L)_{14}$ in the absence of sample. (b) Illustration of reflected pulses from the back surface of the reference surface, front surface of the sample, back surface of the sample, and reflecting metal mirror.

with the Fresnel transmission coefficients given by

$$t_{12}(\nu) = \frac{2}{(1 + n_r(\nu))}, \tag{5}$$

$$t_{21}(\nu) = \frac{2n_r(\nu)}{(n_r(\nu) + 1)}. \tag{6}$$

The attenuation coefficient is given by

$$\alpha = \frac{2\pi\nu n_i}{c}. \tag{7}$$

Birefringence induces a relative phase difference between beams polarized perpendicular to one another transmitted through the material [20]. It can therefore be straightforwardly measured in an experiment similar to that employed to measure sample thickness: specifically, comparison of measurements at two linear polarizations perpendicular to one another reveals a difference in the time-of-flight of terahertz pulse reflections off the front and back surface of the samples. Thus, it is possible to measure the birefringence within a material, whether intrinsic or induced.

Using a rotating wire grid polarizer with $5\,\mu$m tungsten wires at a $12.5\,\mu$m period, reflection measurements were taken on the 3D printed samples at vertical and horizontal polarizations referenced in relation to the print direction, and the arrival times of the reflected pulses were recorded. Since this measurement uses pulse timing, the resulting birefringence is measured at the frequency of maximum power or about 225 GHz. A 25 mm^2 area was scanned in the center of each sample, averaging thirty thousand waveforms for each of the perpendicular polarizations. To present a normalized level of birefringence, $\Delta n/n$ was calculated by

$$\frac{\Delta n}{n} = \frac{t_2 - t_1}{(t_1 + t_2/2)}, \tag{8}$$

where t_1 and t_2 are the timing differences between the front and back surface reflections received at the receiver at the two perpendicular polarizations. This birefringence measurement is composed of the difference in the refractive indices between the two principal axes divided by the average refractive index. This representation allows for a birefringence measurement that is independent of the thickness of the sample and solely dependent on the

birefringent properties of the material. The smaller the value of $\Delta n/n$, the smaller the birefringence present within the printed structure.

3. Results and Discussion

3.1. Uncertainty. The uncertainty in the measured value of the real refractive index at 500 GHz was calculated by differentiating and squaring (1) and then taking an ensemble average (noting that the covariance terms vanish). The uncertainty in the real refractive index is

$$\left(\frac{\sigma_{n_r}}{n_r - 1}\right)^2 = \left(\frac{\sigma_L}{L}\right)^2 + \left(\frac{\sigma_{\phi_s}}{\Delta\phi}\right)^2 + \left(\frac{\sigma_{\phi_r}}{\Delta\phi}\right)^2, \tag{9}$$

where the σ values refer to the standard deviations of the respective measured quantities. The uncertainty in the thickness L and phase difference $\Delta\phi$ was determined by performing the same measurement on a chosen sample 10 times with 1000 waveform averages each, allowing for the calculation of the thickness and phase difference between the reference scan and sample scan 10 times normalized using the central limit theorem. The thickness value L was determined by (2) and its uncertainty by

$$\left(\frac{\sigma_L}{L}\right)^2 = \frac{\left((\sigma t_{14}^o)^2 + \sigma t_{12}^2 + \sigma t_{34}^2\right)}{(t_{14}^o - t_{12} - t_{34})^2}. \tag{10}$$

The uncertainty in the thickness measurements using the ERS was calculated to be 0.6%. Propagation of error using (9) yields a relative uncertainty of 0.3% for the frequency-dependent real refractive index measurements at 500GHz. The attenuation coefficient measurement uncertainty was calculated to be 0.7%. A similar propagation of error analysis was followed for birefringence using (8). This led to a relative uncertainty of 2.7% for the birefringence measurements. A 2 σ threshold (95% confidence interval) will be used to determine if changes in refractive index, attenuation coefficient, and birefringence resulting from variations in the printing parameters are statistically significant.

3.2. Refractive Index Decreases below 200 GHz. For all samples, the calculated refractive index below approximately 200 GHz was observed to decrease with frequency. This phenomenon, seen in the 3D printed samples, was not

present in measurements of various bulk nonprinted plastics. To investigate this difference, samples were printed with varying thicknesses. Using PLA filament, four samples were printed with otherwise identical printing parameters, but thicknesses vary from 2 to 8 mm. The real refractive indices were calculated for these samples: the results are shown in Figure 4 for frequencies below 0.25 THz. Figure 4 shows that decrease below 200 GHz becomes successively less prominent as the thickness of the samples increases. This suggests that a surface roughness effect is responsible, because the relative contribution of the surface roughness will decrease as the thickness increases.

3.3. Real Refractive Indices and Attenuation Coefficients

3.3.1. Material. Figures 5 and 6 show the frequency dependence of the real refractive indices and the attenuation coefficients of the five 3D printing filaments, respectively, for each sample printed with the standard printing parameters described in Section 2.2. The fluctuations in each curve are induced by Fabry-Pérot oscillations; the frequency interval between oscillations is consistent with the thickness of the measured samples. Of particular note is the extremely low value of Polypropylene's attenuation coefficient. The presence of ranges within the curve that trends to an unphysical value below $0 \, cm^{-1}$ indicates that, to properly measure the extremely low attenuation coefficient of Polypropylene in this range, much thicker samples than the ones printed in this research would need to be fabricated. As a consequence, Polypropylene's attenuation coefficients were omitted from the following tables. The attenuation coefficients for PLA and Nylon measured here agree with previously published results, as referenced in Table 1 [12]. Our PC measurement of refractive index was 0.1 higher than that measured in [15]. This could be due to a different chemical formulation of the filaments from differing manufacturers. CPE measurements have not been previously published.

3.3.2. Effect of Printing Parameters on Terahertz Optical Properties. The terahertz optical properties of the materials studied here have previously been demonstrated to be frequency dependent. We chose to isolate and quantify changes in the terahertz optical properties due to variations in printing parameters at a frequency of 500 GHz, chosen for its good signal-to-noise ratio and lack of interference oscillations in the measured data. Tables 3 and 4 show the measured real refractive indices and attenuation coefficients for our samples as their printing parameters are varied. Cura recommended heat and speed settings were used.

As seen in Table 2, as the nozzle size on the printer was increased from 0.4 mm to 0.8 mm, there was a slight consistent increase in the real refractive index in every pair of samples; at an average of 0.33%, this result is not statistically significant as this increase is within the uncertainty of the mean. The attenuation coefficients for PLA, Nylon, and CPE were outside the uncertainty, but no correlation could be drawn between a change in nozzle size and a change in

attenuation coefficient. Therefore, the refractive indices and attenuation coefficients are not correlated with a change in nozzle size.

Table 3 shows the variations caused by changes in layer heights between the samples. Again, the differences measured in refractive index are within the uncertainty. Some materials experience slight increases, while others experience slight decreases, and there is no correlation between layer height and refractive index. Nor is there any correlation with the attenuation coefficients, even though some of the measurements lie outside the calculated uncertainty. To further investigate this result, an additional set of samples were printed, this time with a vertical print orientation rather than a horizontal print orientation. With the print orientation changed, there was still no correlation between layer height and the change in refractive index or attenuation coefficient observed.

Table 4 shows the variation based on changing the print orientation. There was a clear correlation between print orientation and change in refractive index: an average increase of 1.9% in the real refractive index at 500 GHz when the samples were printed horizontally compared to those printed vertically. Three of the four measurable attenuation coefficients had increases greater than the calculated uncertainty. Because air gaps might have caused the change in refractive index, after the measurements were taken, samples were cut and their cross sections were viewed using a light optical microscope, but no air gaps within the prints were discovered. It is, however, plausible that the surface texture differences between the horizontal and vertical samples might cause these correlations. In a vertically printed sample, the terahertz beam is interacting with a repeating structure surface layer with features of similar size to its wavelength. It has been previously reported that increasing the surface roughness of various samples measured in the terahertz range increases the uncertainty of thickness measurements as well as increasing the measured values of real refractive indices [21, 22].

3.3.3. Intrinsic Birefringence. Horizontally printed samples showed birefringence levels below the calculated uncertainty in the measurement. Vertically printed samples however showed birefringence levels above the uncertainty; accordingly, only these latter values are presented. The lack of measurable birefringence in the horizontally printed samples is plausibly due to the cancellation of any induced stresses in the rasters during printing because of the cross-hatch pattern that is performed while printing in this direction. This cross-hatch pattern is perpendicular to the terahertz beam during transmission, and therefore all opposing layers' stresses will be effectively nulled during the phase change. As shown in Figure 7, as the layer height of the samples increases, using both a 0.4 mm and 0.8 mm nozzles, the birefringence present in the sample also increases. This trend was seen in every filament material.

Additional stresses may be induced into the material as it is rapidly heated and cooled from printing temperature back to room temperature during the FDM 3D printing process.
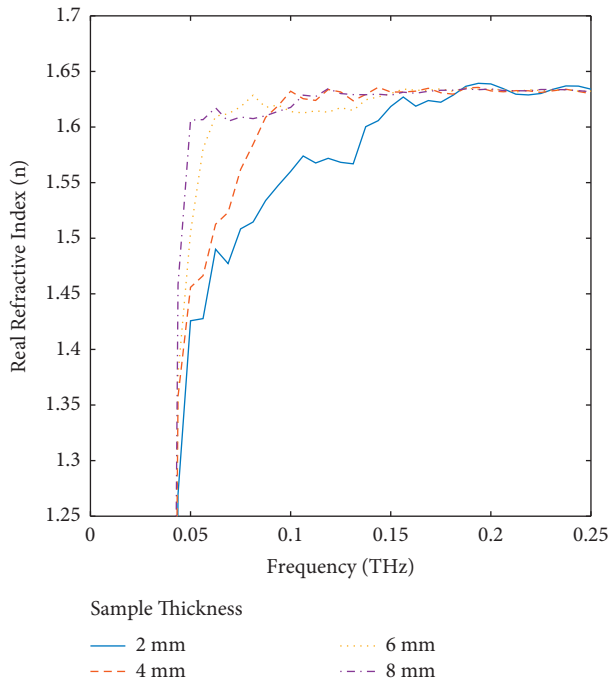
FIGURE 4: Extracted frequency-dependent refractive index drop-off below 200 GHz. As the thickness of the printed samples increases, the effect of the drop-off decreases. Data below 0.05 THz would be unreliable because of negligible detectable signal.

FIGURE 6: Extracted frequency-dependent attenuation coefficients of the five 3D printing filaments used in this research measured using electric field.
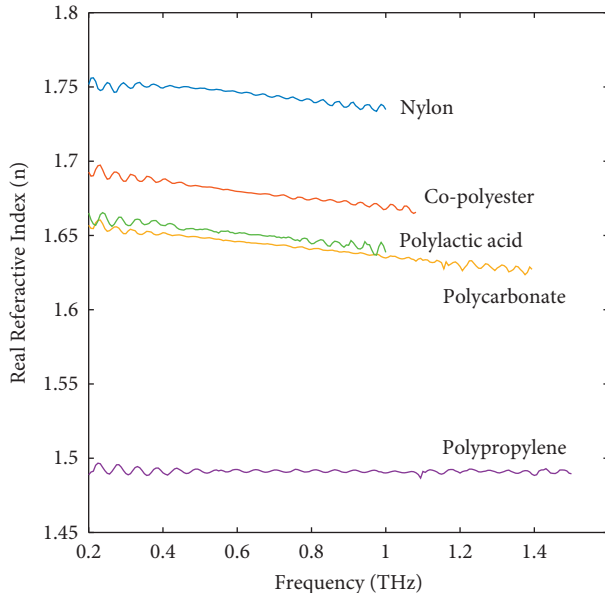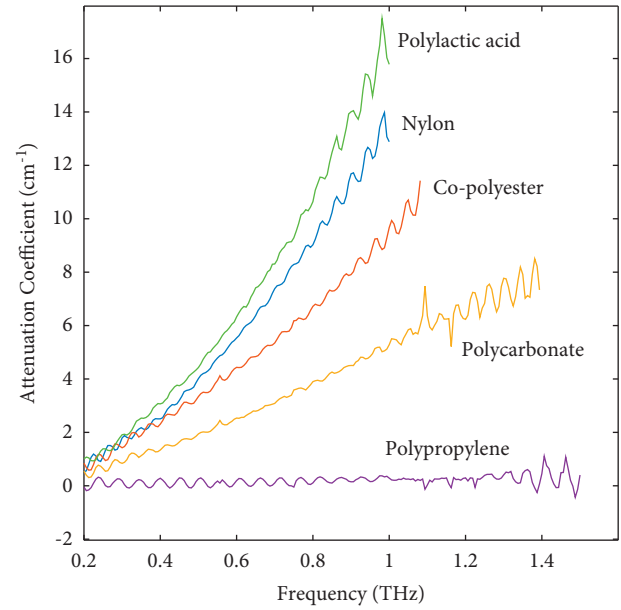

FIGURE 5: Extracted frequency-dependent refractive indices of the five 3D printing filaments used in this research.

These large thermal fluctuations combined with forced extrusion could create a birefringence within the final structure as the layers are deposited on top of one another. As seen in Figure 7, the increase in nozzle size from (a) 0.4 mm to (b) 0.8 mm caused an average of 125% decrease in birefringence. One possible explanation for this decrease is that with the larger nozzle size each layer of the sample is printed faster and, since each layer is printed faster, there is less elapsed time for that layer to cool, decreasing the introduction of residual stresses into the material due to thermal differences between layers. Consequential thermal differences between layers would create larger measurable birefringence, such as those seen in the slower printing 0.4 mm nozzle samples.

3.4. Discussion. Previous studies on terahertz characterization of 3D printed structures such as Squires and Lewis (2018) print various filaments under the so-called optimal printing conditions of printing temperature and printing speed. The terahertz refractive index and absorption coefficient are characterized for the optimally printed structures. While Squires and Lewis (2018) only varied the composition of the FDM filaments, this paper has a different emphasis: Do the printing parameters such as nozzle size, layer height, and orientation *change* the terahertz refractive index, absorption coefficient, and birefringence of the optimally printed structures? The printing temperature and printing speed are not varied in this paper. Recommended settings from the filament/printer manufacturer for optimal printing were used. However, the nozzle size, layer height, and orientation are not typically recommended by filament or printer manufacturers. These printing parameters are typically chosen by the user depending on the desired results of the printed part.

In this paper, 3D printed samples were designed and fabricated with the intent to observe any changes in the printed materials of real refractive index, attenuation coefficient, and birefringence. Horizontally printed samples have an average of a 1.9% increase in real refractive index over vertically printed samples, alongside lower attenuation

TABLE 2: Real refractive indices and attenuation coefficients at 500 GHz based on variation in printer's nozzle size. Standard printing parameters of a 0.2 mm layer height and a horizontal printing orientation were used. Uncertainties in the real refractive index: $2\sigma = \pm 0.010$; attenuation coefficient: $2\sigma = \pm 0.025$.

Filament material	Nozzle size (mm)	Real refractive index (n)	Attenuation coefficient (cm^{-1})
PLA	0.4	1.654	4.429
	0.8	1.657	4.587
Nylon	0.4	1.749	4.015
	0.8	1.758	3.921
PC	0.4	1.649	1.944
	0.8	1.654	1.924
CPE	0.4	1.683	3.343
	0.8	1.691	3.461
PP	0.4	1.492	N/A
	0.8	1.495	N/A

TABLE 3: Real refractive indices and attenuation coefficients at 500 GHz based on variation in the print's layer height. Standard printing parameters of a 0.4 mm nozzle and a horizontal printing orientation were used. Uncertainties in the real refractive index: $2\sigma = \pm 0.010$; attenuation coefficient: $2\sigma = \pm 0.025$.

Filament material	Layer height (mm)	Real refractive index (n)	Attenuation coefficient (cm^{-1})
PLA	0.1	1.658	4.455
	0.2	1.654	4.429
	0.3	1.641	4.543
Nylon	0.1	1.755	3.961
	0.2	1.749	4.015
	0.3	1.753	4.020
PC	0.1	1.663	2.104
	0.2	1.649	1.944
	0.3	1.663	2.123
CPE	0.1	1.689	3.161
	0.2	1.683	3.343
	0.3	1.670	3.675
PP	0.1	1.493	N/A
	0.2	1.492	N/A
	0.3	1.492	N/A

TABLE 4: Real refractive indices and attenuation coefficients of samples at 500 GHz based on variation in print orientation. Standard printing parameters of a 0.4 mm nozzle and 0.2 mm layer heights were used. Uncertainties in the real refractive index: $2\sigma = \pm 0.010$; attenuation coefficient: $2\sigma = \pm 0.025$.

Filament material	Print orientation	Real refractive index (n)	Attenuation coefficient (cm^{-1})
PLA	Horizontal	1.654	4.429
	Vertical	1.604	5.092
Nylon	Horizontal	1.749	4.015
	Vertical	1.741	4.099
PC	Horizontal	1.649	1.944
	Vertical	1.623	2.444
CPE	Horizontal	1.683	3.343
	Vertical	1.650	3.191
PP	Horizontal	1.492	N/A
	Vertical	1.457	N/A

coefficients for three of the four measurable filament materials, while only vertically printed samples had measurable birefringence. These changes are notably greater than the calculated relative uncertainties in refractive index and attenuation coefficient at 500 GHz of 0.3% and 0.7%, respectively. With an increase in nozzle size from 0.4 mm to 0.8 mm, there was an average increase of 0.33% in refractive index across all samples, but these measurements are within the calculated uncertainty (2σ) from the mean. An overall average decrease of 125% in birefringence was measured with an increase in nozzle size from 0.4 mm to 0.8 mm. No correlation between attenuation coefficient and nozzle size was found. There was no direct correlation between layer height and change in refractive index or attenuation
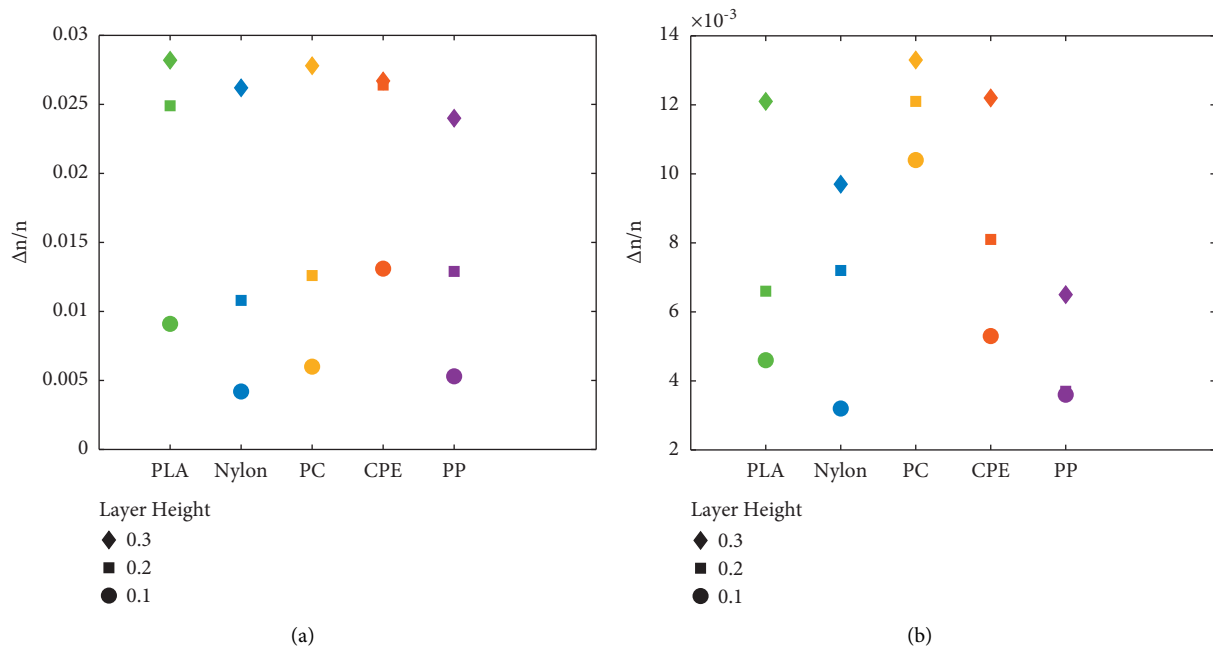
(a)

(b)

FIGURE 7: Level of birefringence ($\Delta n/n$) measured at 250 GHz in vertically printed samples using (a) 0.4 mm and (b) 0.8 mm nozzle with variation of print layer height.

coefficient, but there was a clear trend that increasing layer height at the tested intervals caused an increase in the birefringence present within the samples.

It is important to know if 3D printing parameters alter the terahertz refractive index and attenuation of printed components. If the terahertz refractive index, attenuation coefficient, or birefringence were to change with printing parameters, designers would need to take that into account in fabricating the type of terahertz devices summarized in Squires and Lewis (2018). As an example, if the refractive index of a 3D printed terahertz lens varies with printing parameters, then the focal length of the lens would be dependent on printing parameters. Likewise, if the attenuation depended on printing parameters, then the throughput transmission of the lens would be dependent on the printing parameters as well. Similarly, if the refractive index, attenuation coefficient, or birefringence of a printed terahertz waveguide were to vary due to printing parameters, then the device performance (e.g., propagation speed of guided terahertz, numerical aperture of the waveguide, and loss per unit length of the waveguide) would all be dependent on the various printing parameters.

Even if the 3D printed components were not going to be used as terahertz device components, it would still be important to understand how the terahertz optical properties change with printing parameters. It is well known in additive manufacturing that qualification and validation of 3D printed component shapes, dimensions, mechanical strength, etc., are an important issue [7–11]. Clearly, if one were trying to measure the thickness of 3D printed layers, using the time delay of terahertz pulses through the material as an NDE method to determine the thickness via time-of-flight, depends on the refractive index of the material. If the

refractive index were to vary with print parameters, then it is possible that a variation in terahertz refractive index due to printing parameters might be misinterpreted as a thickness variation in the printed component, with a collateral introduction of birefringence into the measured structure. While the work presented in this paper focuses on FDM printing of certain plastics, the same terahertz techniques could be used to qualify ceramic 3D printed components, as well as the vast array of additive manufacturing materials and techniques transparent to terahertz radiation.

4. Conclusions

The goal of this paper is to determine the degree to which 3D printing parameters change the terahertz refractive index, attenuation, and birefringence. If variations in the printing parameters alter the terahertz optical properties, this would lead to variations in the performance of 3D printed device components as well as potential misinterpretation of terahertz NDE of 3D printed components. Based on these results, depending on the degree of precision in the refractive index, attenuation coefficient, and birefringence needed, performance variations in FDM 3D printed structures that rely on tailored optical properties such as various microwave and terahertz based optical components including lenses, waveguides, and antennas should therefore take into consideration changing certain printing parameters during the fabrication process. Nozzle size and layer height are not correlated to changes in refractive index and attenuation coefficient, effectively reducing the parameters of concern for these tailored characteristics, unlike the birefringence of the structure, while notably print orientation has a measurable effect on all three optical properties. The

methodology described here also provides a foundation for nondestructive evaluation of FDM 3D printed objects and structures.

Data Availability

The data used in this paper can be made available upon request to Alexander Clark, aclark2@njit.edu.

Conflicts of Interest

The authors declare that there are no conflicts of interest regarding the publication of this paper.

Acknowledgments

References

[1] S. Wang and X.-C. Zhang, "Pulsed terahertz tomography," *Journal of Physics D: Applied Physics*, vol. 37, no. 4, pp. R1–R36, 2004.

[2] K. Chen, D. Xu, J. Li, X. Geng, K. Zhong, and J. Yao, "Application of terahertz time-domain spectroscopy in atmospheric pressure plasma jet diagnosis," *Results in Physics*, vol. 16, Article ID 102928, 2020.

[3] C. R. Nicoletti, L. Cramer, A. Fletcher, D. Zimdars, Z. Iqbal, and J. F. Federici, "Non-destructive evaluation of specialty coating degradation Using terahertz time-domain spectroscopy," *Proceedings of SPIE*, vol. 10206, Article ID 102060W, 2017.

[4] H. Chen, X. Chen, S. Ma et al., "Quantify glucose level in freshly diabetic's blood by terahertz time-domain spectroscopy," *Journal of Infrared, Millimeter and Terahertz Waves*, vol. 39, no. 4, pp. 399–408, 2018.

[5] W. J. Otter and S. Lucyszyn, "3-D printing of microwave components for 21st century applications," in *Proceedings of the 2016 IEEE MTT-S International Microwave Workshop Series on Advanced Materials and Processes for RF and THz Applications (IMWS-AMP)*, IEEE, Chengdu, China, July 2016.

[6] S. Yang, X. Sheng, G. Zhao, S. Lou, and J. Guo, "3D printed effective single-mode terahertz antiresonant hollow core fiber," *IEEE Access*, vol. 9, pp. 29599–29608, 2021.

[7] E. George, P. Liacouras, F. J. Rybicki, and D. Mitsouras, "Measuring and establishing the accuracy and reproducibility of 3d Printed Medical models," *RadioGraphics*, vol. 37, no. 5, pp. 1424–1450, 2017.

[8] T. AlGeddawy and H. ElMaraghy, "Product variety management in design and manufacturing: challenges and strategies," in *Enabling Manufacturing Competitiveness and Economic Sustainability*, H. ElMaraghy, Ed., Springer, Berlin, Heidelberg, pp. 518–523, September 2011.

[9] I. Wing, R. Gorham, and B. Sniderman, "3D opportunity for quality assurance and parts qualification," 2015, https://www2.deloitte.com/insights/us/en/focus/3d-opportunity/3d-printing-quality-assurance-in-manufacturing.html.

[10] US Government Accountability Office report to the chairman, "Committee on science, space, and technology, house of representatives," 3D printing: Opportunities, challenges, and policy implications of additive manufacturing, 2015, http://www.gao.gov/assets/680/670960.pdf.

[11] C. K. Chua, C. H. Wong, and W. Y. Yeong, "Equipment qualification," in *Standards, Quality Control, and Measurement Sciences in 3D Printing and Additive Manufacturing*, pp. 139–157, Academic Press, London, 2017.

[12] S. F. Busch, M. Weidenbach, M. Fey, F. Schäfer, T. Probst, and M. Koch, "Optical properties of 3D printable plastics in the THz regime and their application for 3D printed THz optics," *Journal of Infrared, Millimeter and Terahertz Waves*, vol. 35, no. 12, pp. 993–997, 2014.

[13] M. Scheller, "Data extraction from terahertz time domain spectroscopy measurements," *Journal of Infrared, Millimeter and Terahertz Waves*, vol. 35, no. 8, pp. 638–648, 2014.

[14] A. D. Squires, E. Constable, and R. A. Lewis, "3D printed terahertz diffraction gratings and lenses," *Journal of Infrared, Millimeter and Terahertz Waves*, vol. 36, no. 1, pp. 72–80, 2014.

[15] A. D. Squires and R. A. Lewis, "Feasibility and characterization of common and exotic filaments for use in 3d printed terahertz devices," *Journal of Infrared, Millimeter and Terahertz Waves*, vol. 39, no. 7, pp. 614–635, 2018.

[16] J. A. Colla, R. E. M. Vickers, M. Nancarrow, and R. A. Lewis, "3D printing metallised plastics as terahertz reflectors," *Journal of Infrared, Millimeter and Terahertz Waves*, vol. 40, no. 7, pp. 752–762, 2019.

[17] J. S. White, D. Zimdars, and I. Duling, "Very high speed THz imaging of foam density and other defects," in *Proceedings of the 2016 41st International Conference on Infrared, Millimeter, and Terahertz Waves (IRMMW-THz)*, IEEE, Copenhagen, Denmark, September 2016.

[18] M. Bernier, F. Garet, and J.-L. Coutaz, "Determining the complex refractive index of materials in the far-infrared from terahertz time-domain data," *Terahertz Spectroscopy - A Cutting Edge Technology*, Books on Demand, Nordstedt, Germany, 2017.

[19] S. S. Prabhu, "Terahertz spectroscopy," in *Molecular and Laser Spectroscopy: Advances and Applications*, V. P. Gupta, Ed., Elsevier, pp. 65–85, Amsterdam, Netherlands, 2018.

[20] V. Ganapati, S. Schoenfelder, S. Castellanos et al., "Infrared birefringence imaging of residual stress and bulk defects in multicrystalline silicon," *Journal of Applied Physics*, vol. 108, no. 6, Article ID 063528, 2010.

[21] R. Burger, J. Frisch, M. Hübner et al., "THz-TDS reflection measurement of coating thicknesses at non-perpendicular incidence: experiment and simulation," *Sensors*, vol. 21, no. 10, p. 3473, 2021.

[22] T. Fukuchi, N. Fuse, M. Mizuno, and K. Fukunaga, "THz measurement of refractive index and thickness of ceramic coating on a metal substrate," in *Proceedings of the 2013 Conference on Lasers and Electro-Optics Pacific Rim (CLEOPR)*, IEEE, Kyoto, Japan, June 2013.